Enhancing Reliability of Chromogenic Bioassay with Two-Electron TMB Oxidation Enabled by Self-assembled Surfactants Nanozyme

Caixia Zhu, Yuan Xu, Qing Hong, Xuwen Cao, Kaiyuan Wang, Yanfei Shen, Songqin Liu, Yuanjian Zhang*

Jiangsu Engineering Laboratory of Smart Carbon-Rich Materials and Device, Jiangsu Province Hi-Tech Key Laboratory for Bio-Medical Research, State Key Laboratory of Bioelectronics, School of Chemistry and Chemical Engineering, Medical School, Southeast University, Nanjing 21189, China. Email: Yuanjian.Zhang@seu.edu.cn

Abstract

In a standard colorimetric sensing assay based on HRP-H_2O_2-TMB (3,3',5,5'-tetramethylbenzidine), the stability of the signal of the chromogenic probe (TMB_{ox}) is essential for the accuracy of measurements. Terminators, typically of strong acids, are often added to maintain signal stability. However, additional manipulations may compromise sensing accuracy and the use of strong acids cause safety hazards. Here, a self-assembled sodium dodecyl sulfate (SDS) micellar nanozymes sensing strategy was proposed, which can catalyze the two-electron oxidization of TMB directly to the final state. Unlike the free and bound oxygen intermediates pathways, the micellar nanozymes enabled a microenvironment conducive to two-electron oxidization of TMB, in which the electrostatic attraction between the micellar nanozymes and TMB played crucial roles in substrate activation and intermediates stabilization. It allows micellar nanozyme to remain active even at very high H_2O_2 concentrations, thus enabling a broader detection range. GOD and the micellar nanozymes were cascaded for glucose detection as an application. As a result, the disadvantage of signal instability in conventional glucose biosensors from natural enzyme systems (HRP and GOD) was avoided.

Keywords: micelles, nanozymes, TMB, reliability, glucose biosensors

Introduction

Catalysts were widely used to promote the reaction's speed, efficiency, and selectivity. Among them, enzymes as natural catalysts have been described as the "chip" of modern biocatalytic reactions, which play an essential role in many practical applications, such as bioassay, food, medicine, and industrial catalysis.[1-2] Among them, peroxidases are a class of oxidoreductase extracted from living organisms, which takes heme as a cofactor to participate in the physiological metabolism of organisms.[3] It could catalyze the oxidation of various substrates by reacting with H_2O_2 to form a high-valent iron oxide intermediate.[4-5] As a typical representative, horseradish peroxidase (HRP) has been widely used in analytical chemistry and immunochemistry due to its high catalytic efficiency, specificity, and mild reaction conditions.[6-9] For instance, HRP-H_2O_2-TMB (3,3',5,5'-tetramethylbenzidine) has become the standard chromogenic system in the commonly used enzyme-linked immunosorbent assay (ELISA). However, enzymes are generally easy to denature in vitro, and enzyme purification is laborious and costly, which impedes their broad application. Moreover, some enzyme-catalyzed system has intrinsic limitations in reactivity. Building on the prior example, the continuous re-oxidation of one-electron oxidation product (TMB_{ox1}) to its final state (TMB_{ox2}) by HRP is inevitable. To improve the stability and reliability of signal, adding a terminator, typically of strong acid, to the HRP-H_2O_2-TMB system is generally needed.[10-12] However, with that, will come corrosion, causing critical safety hazards in applications. Therefore, there is an urgent need to develop artificial enzymes to address these challenges.

Indeed, the long-term stability of TMB_{ox2} motivates us to consider whether an artificial enzyme could be developed to catalyze the oxidization of TMB directly to the final state TMB_{ox2}. Since the first discovery of Fe_3O_4 nanoparticles with intrinsic peroxidase (POD)-like activity in 2007, many nanomaterials-based artificial enzymes, termed nanozymes, have been reported.[13-15] Due to low cost, easy availability, and high stability against biodegradation, nanozymes have attracted increasing attention in a wide range of fields, such as biosensors, immunoassays, and cancer therapy.[16-19] Likewise, bottom-up self-assembled artificial enzymes have recently attracted much attention.[20-22] Biomolecules such as DNA and peptides have unique molecular structures and, as assembly elements, were often used to prepare aggregates with controllable morphology and catalytic function.[21, 23-25] However, artificial enzymes

constructed using these biomolecules cannot avoid the intrinsic disadvantages of poor stability. Surfactants with unique molecular structures may become the most appropriate assembly elements for self-assembling artificial enzymes.[26-28] Surfactants can acquire potential enzyme-like active sites through self-assembly and bind to substrates through hydrogen bonding, van der Waals forces, or hydrophobic interactions to form a substrate activation state, ultimately facilitating the reaction of the substrate.[29-30] Moreover, micelles could solubilize many substances in an aqueous solution, thus catalyzing reactions by using the solubilization, stabilization, and sensitization of micelle systems.[31-32] Therefore, we reason that developing a micellar nanozyme would provide a potential benign solution for addressing the instability of TMB oxidation in bioassay by HRP. However, to our knowledge, few relevant studies have been reported.

Here, we developed a micellar nanozyme to directly oxidize TMB to the stable final state, TMB_{ox2}, for sensing applications, thanks to the interaction between micellar nanozymes and substrates. The unique POD-like activity of sodium dodecyl sulfate (SDS) -based micellar nanozymes was discussed, considering the catalytic reaction of TMB oxidation as an example. The critical factors of micelle-substrate interactions were explored to understand the origin of the stable catalytic ability. The special catalytic mechanism allows micellar enzymes to remain active even at very high H_2O_2 concentrations, thus enabling the detection of ultra-high H_2O_2 concentrations. Interestingly, the stability of the SDS micellar nanozymes for the two-electron oxidation product (TMB_{ox2}) ensured the uniqueness of the final chromogenic signal. As a result, without HRP, glucose could be reliably measured with an SDS-based micellar nanozyme-H_2O_2-TMB chromogenic system without any strong acid termination.

Results and discussion

The two-electron oxidation of TMB. As a common surfactant, SDS has been successfully used as a catalyst in many organic reactions because it can form water micelles and dissolve water-insoluble organic compounds[33]. Inspired by the fact, SDS micellar nanozymes were applied as a proof-of-concept to verify the feasibility of constructing micellar nanozymes by improving the reaction rate in the dehydrogenation of TMB. As shown in Figure 1a, an increase in the absorbance at 450 nm was observed, which was attributed to the two-electron oxidation of TMB into yellow TMB_{ox2} by the SDS micellar nanozymes with H_2O_2. The oxidation rate of TMB by H_2O_2 increased

significantly upon adding SDS micelles (Figure S1). The results demonstrated that the SDS micellar nanozymes had POD-like activity and could catalyze the oxidation of TMB with H_2O_2 in an aqueous solution. The TMB oxidation rate was calculated from the absorbance of TMB_{ox2} as a function of time. It was found that the steady-state kinetics for the SDS micelle catalytic reaction well followed the typical Michaelis-Menten model (Figure 1b).

To validate the products of the catalytic reaction, the substrate and oxidation product of TMB in the solution phase were explored using high-resolution electrospray ionization mass spectrometry (ESI-MS, Figure 1c, bottom panel). Before oxidation, a fragment of TMB ([M + H]) was observed at m/z 241.1706. However, the fragment was exclusively downshifted to 239.0278 after oxidation. It demonstrated the dehydrogenation of the two -NH moieties on TMB and the oxidation of TMB into TMB_{ox2}. The high-performance liquid chromatography (HPLC) chromatogram (Figure S2) also showed that the product of TMB catalyzed by SDS micellar nanozymes was TMB_{ox2}, similar to the yellow product obtained from HRP oxidation. The results suggested that the SDS micellar nanozyme not only accelerated the oxidation reaction of TMB in the presence of H_2O_2 but also produced the final oxidation product of TMB, namely the two-electron oxidation product. In fact, during the catalytic reactions of natural and artificial peroxidases, the catalytic oxidation of TMB was generally converted into a one-electron oxidation product. Then the generated one-electron product was slowly oxidized to the terminated product, which leads to instability of the output signal in constructing biosensors. For instance, additional terminators were added in the ELISA experiments to avoid unfavorable signal changes for readings. In contrast, the catalytic oxidation of TMB by SDS micellar nanozyme provided direct access to the final state. It generated TMB_{ox2} much faster than HRP and Pt/C by a factor of three to five times (Figure 1d). Forming a unique catalytic product is essential for successfully constructing reliable biosensors, which will be demonstrated in the following text using the proposed SDS micellar nanozyme.

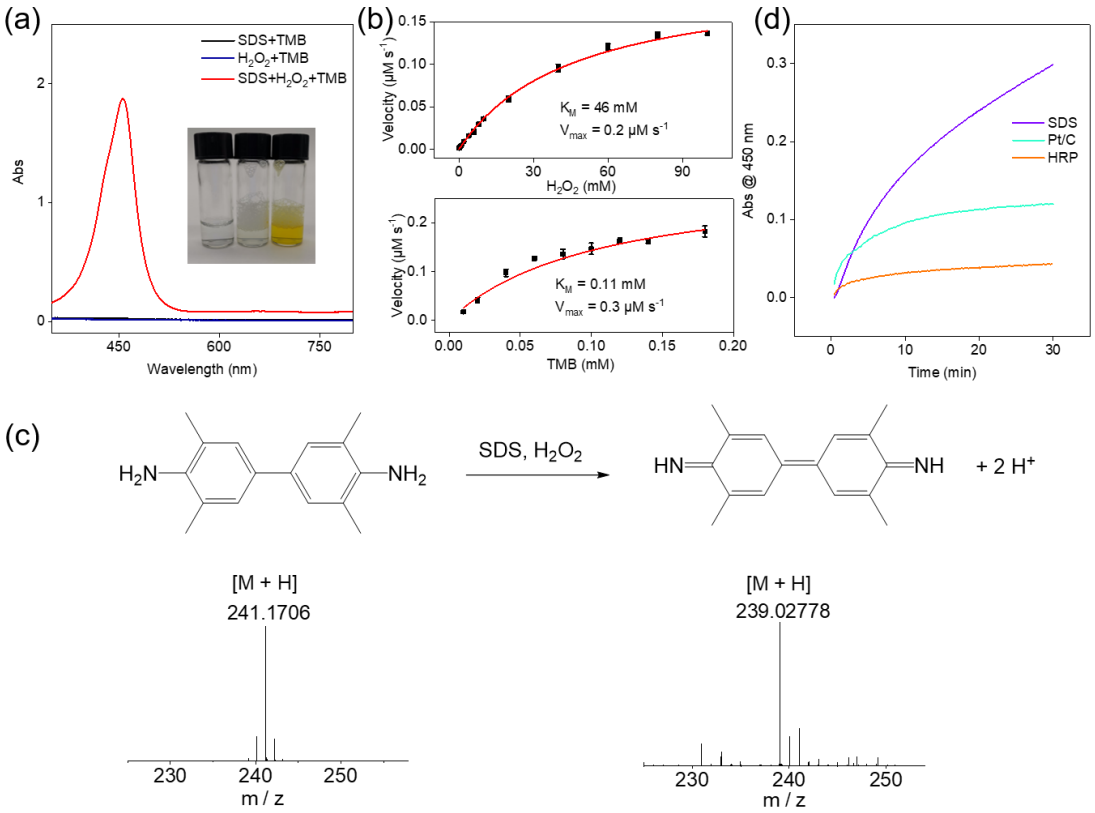

Figure 1. Catalytic activity of SDS micellar nanozymes. (a) UV-vis absorption spectra of TMB (0.1 mM) after catalysis by SDS micellar nanozymes (10 mM) in air-saturated 0.1 M HAc-NaAc buffer solution ([H_2O_2]: 0.1 M). (b) The typical Michaelis-Menten curves for 10 mM SDS with TMB ([H_2O_2]: 0.1 M) and H_2O_2 ([TMB]: 1 mM) as substrate in 0.1 M HAc-NaAc (pH 3.5), respectively. (c) Reaction pathway of TMB oxidation catalyzed by SDS micellar nanozymes (10 mM), as evidenced by ESI-MS spectra of TMB and TMB_{ox2}. (d) Time-dependent UV-vis absorption of TMB at 450 nm catalyzed by SDS micellar nanozymes, Pt/C, and HRP in air-saturated 0.1 M HAc-NaAc buffer solution ([H_2O_2]: 10 μM).

Mechanism of two-electron oxidation of TMB. To understand the mechanism by which SDS micellar nanozyme accelerated the electron exchange between TMB and H_2O_2, possible intermediate radical species, such as free reactive oxygen species (ROS), were first explored using the scavenger trapping technique. UV-vis kinetic experiments were performed using isopropyl alcohol (IPA) as a hydroxyl radical scavenger (Figure 2a). It was observed that the oxidation rate of TMB decreased dramatically after adding IPA, confirming that hydroxyl radicals were the primary radical intermediates in the reaction process.[34] Moreover, the oxidation products increased with the amount of

hydroxyl radicals, which positively correlated with the H_2O_2 concentration in the solution (Figure S3, S4). Electron spin resonance (ESR) spectra were carried out to further confirm the type of ROS by monitoring the effect of SDS micelle addition on the generation of free radicals in the H_2O_2 solution (Figure 2b-2e). As shown in Figure 2b, using 5,5-dimethyl-1-pyrroline N-oxide (DMPO) as the spin-trapping agent, distinct 4-fold characteristic peaks of hydroxyl radical-DMPO adducts with a signal intensity of 1:2:2:1 were observed both before and after the addition of SDS micellar nanozymes. The signal intensities of the solutions before and after SDS addition were equal, indicating that the hydroxyl radicals originating from the self-decomposition of H_2O_2 and the addition of SDS micellar nanozymes did not increase the efficiency of hydroxyl radical production (Figure 2b and c). The results suggested that the catalytic mechanism of SDS micellar nanozyme did not follow the pathway of activating H_2O_2 to form the free ROS.[4, 35-36]

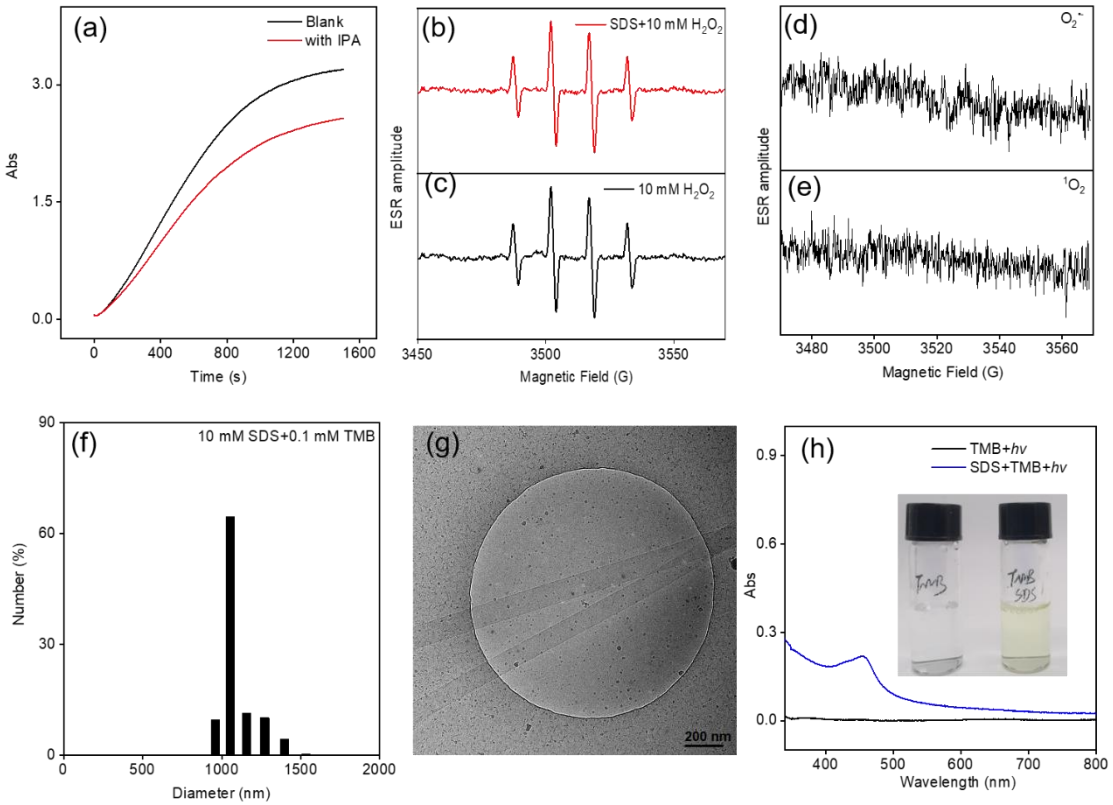

Figure 2. Intermediates in peroxidase-like reactions by SDS micellar nanozyme. (a) Time-dependent UV-vis absorption of TMB catalyzed by SDS micellar nanozymes (10 mM) with or without IPA as the hydroxyl radical trapping agent. ESR spectra of the spin adduct of the hydroxyl radical generated by H_2O_2 before (b) and after (c) the addition of SDS micellar nanozymes. ESR spectra of spin adduct of superoxide radical (d) and singlet oxygen (e) generated by H_2O_2 in 0.1 M HAc-NaAc solution. (f) DLS

size distributions of SDS micelles addition of TMB. (g) Cryo-TEM images of SDS micelles (10 mM) after addition of TMB (0.1 mM). (h) UV-vis absorption spectra of TMB after irradiation with visible light ($\lambda \geq 400$ nm) in solutions with or without the addition of SDS micellar nanozymes (10 mM).

Previous studies on micellar catalysis have shown that the micellar microenvironment can change the state of the substrate or transition state, thereby affecting the reaction progress.[30, 37-38] Next, the interactions between the micellar nanozymes and TMB in bimolecular reactions were investigated. The sizes of the particles in SDS micellar solutions before and after TMB addition were measured by dynamic light scattering (DLS). As can be seen from Figure S5, the micelle size in pure SDS solution was approximately 4 nm, which was consistent with the values reported in the literature.[39-40] However, the micelle size increased dramatically to about 1000 nm with the addition of TMB (Figure 2f). When SDS was dissolved in pure water, there was a high degree of electrostatic repulsion between the head clusters in the micelles, owing to the negative charge of the anion head clusters. It led to a sizeable effective head cluster area and a high micelle core curvature, resulting in spherical micelles forming. In fact, at concentrations much higher than the critical micelle concentration (CMC) or with additives, the micelles would undergo a morphological transformation into a cylindrical structure with a 100-1000 nm length.[40-41] The transformation was caused by reducing the effective area of the head cluster or by reducing the electrostatic repulsion. The transformation has been demonstrated experimentally and by all-atom molecular dynamics simulation studies of micelle front aggregation.[40, 42]

To determine the specific structure of the micelles in the mixed TMB and SDS system, cryo-TEM imaging was performed, showing a cylindrical form (Figure 2g). The results confirmed that the addition of TMB caused a morphological change in the micelles, which may be due to van der Waals forces and hydrophobic interactions. It can be assumed that the special intermediate state formed by TMB and the micellar nanozymes, which made TMB seem to be in an “activated state” and made it easier for oxidative dehydrogenation. Figure 2h shows a comparison of the results of oxidized product of TMB with and without SDS micellar nanozymes under visible-light irradiation ($\lambda \geq 400$ nm). The results showed that the introduction of SDS micellar nanozymes significantly affected on the rapid dehydrogenation of TMB. It was demonstrated that “activated state” formed readily allowed the oxidation of TMB, i.e., activated TMB. No UV light

was required and low-energy light illumination allowed the reaction to occur. It has been demonstrated that micelles have solubilizing effects and can promote catalysis by binding to the substrate through hydrogen bonding, van der Waals forces, or electrostatic gravitational forces.[29-32] In addition, micelle aggregates of nanometer dimensions behaved as containers in which a variety of reactions occur. Nanometer-sized micelles increased the local concentration of reactants around their surfaces, which was also one of the reasons for the accelerated transformation. Therefore, in contrast to traditional peroxidase's mechanism in activating H_2O_2, micellar nanozymes accelerated the oxidative dehydrogenation process via TMB activation.

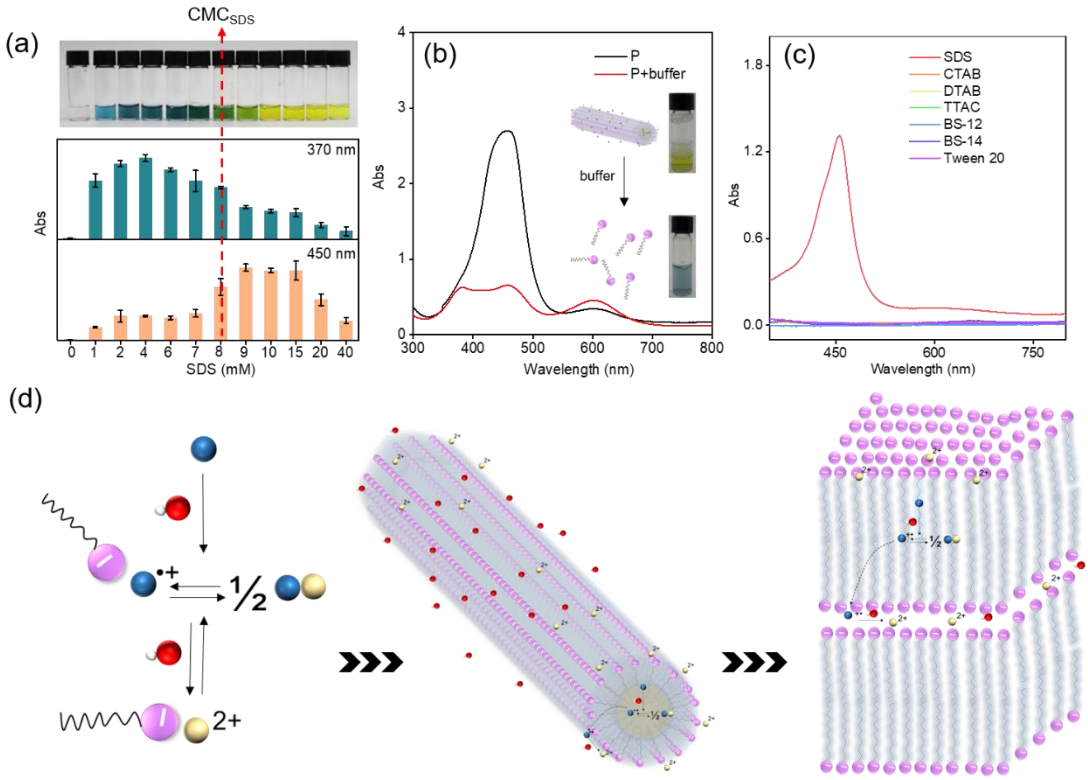

Figure 3. Mechanistic studies of the POD-like activity. (a) Color (top panel) and UV-vis absorption (bottom panel) changes in the oxidation solution of TMB with increasing SDS concentrations. (b) UV-vis absorption spectra of P solution before and after the addition of and SDS micelle solution. (The P solution was obtained by oxidation of TMB catalyzed by SDS micellar nanozymes (10 mM) in the presence of H_2O_2). (c) The catalytic activity of different surfactants for TMB oxidation, as measured by UV-vis spectroscopy. (The concentration of each surfactant used in the experiment was the critical micelle concentration) (d) The proposed bound TMB mechanism for SDS micellar nanozymes.

To confirm the role of micelles on the catalysis process, the influence of different concentrations of SDS on the catalytic reaction was studied. Figure S6 shows the mechanism of the oxidation of TMB to produce two colored products. As shown in Figure 3a (top panel), with increasing SDS concentration, the color of the products gradually changed from blue to yellow. The inflection point of the product transition corresponded to the critical micelle concentration of SDS (8 mM). The UV-vis spectra corresponding to each concentration of the solution also confirmed the transformation of the products (Figure S7). To make the data more intuitive, Figure 3a (bottom panel) shows the trend plots of the blue product (370 nm, one-electron oxidation product) and yellow product (450 nm, two-electron oxidation product) with increasing SDS concentration. The results showed that the addition of different concentrations of SDS accelerated the oxidation of TMB in the presence of H_2O_2 compared to samples without SDS. With an increase in SDS concentration, the oxidation products gradually changed from the one-electron oxidation product to the two-electron oxidation product.

Next, the effect of micelles on the catalytic reaction process in our proposed catalytic mechanism was verified. First, an equal volume of buffer was introduced into the product solution (P refers to the product solution of TMB after catalysis by the SDS micellar nanozymes). The change in absorbance was measured using UV-vis spectroscopy. As shown in Figure 3b, compared with the UV-vis absorption spectra of the original product solution (P), the absorbance of the two-electron products (450 nm) decreased; meanwhile, that of one-electron products (600 nm) increased after 1 mL of HAc-NaAc buffer (pH 3.5, 0.1 M) was added to 1 mL of P solution. The change was because adding the buffer diluted the original solution and destroyed the original micelle structure. The TMB molecules encapsulated in the micelles were released, and the blue one-electron oxidation product of TMB was obtained again through reaction Equation 4.

For comparison, 1 mL of SDS micelle (10 mM) solution was added to 1 mL of the P solution. In the case, the SDS concentration in the solution was kept constant. As shown in Figure S8, a decrease in the absorbance of two-electron products (450 nm) was

observed, but there was no increase in the absorbance of one-electron products (600 nm). Consistently, the color of the solution did not turn blue but only became lighter (Figure S8, inset). It was confirmed that the micellar structure was more favorable for stabilizing the two-electron oxidation product TMB_{ox2}. In addition, TMB_{ox2} when the amount of TMB_{ox2} exceeded the maximum amount that SDS micellar nanozyme could stabilize, one-electron products gradually appeared in the solution (Figure 9, see Supporting Information for more details). These results confirmed the important role of micelle structure on the catalysis process.

It is well known that there is an electrostatic gravitational force between the positive and negative charges.[43-45] In fact, the TMB oxidation products are positively charged, and SDS is an anionic surfactant with a negative charge. Therefore, the role of the electrostatic effect between the micelle and the substrate on the catalytic effect is also worth exploring. As a comparison, cationic surfactants (e.g., cetyltrimethylammonium bromide, CTAB; dodecyltrimethylammonium bromide, DTAB; tetradecyltrimethylammonium chloride, TTAC) were firstly explored. As expected, only SDS micellar nanozymes showed a catalytic acceleration of the reaction between H_2O_2 and TMB (Figure 3c). Second, the results that SDS micellar nanozymes could catalyze other positively charged chromogenic substrates, which further confirmed the vital role of electrostatic attraction in micellar nanozymes catalysis (Figures S10). Third, the role of the electrostatic effect was further demonstrated by the phenomenon that cationic micelles can catalyze the oxidation of negatively charged substrates (Figures S11). In the sense, the electrostatic interactions between SDS micellar nanozymes and TMB was also play an important role.

Based on these considerations, we proposed a possible mechanism by which SDS promotes the reaction of TMB with H_2O_2. As shown in Equation (1) – (4), the TMB oxidation reaction was in equilibrium with both one-electron oxidation products TMB_{ox1} ($TMB^{\bullet+}$ and charge transfer complexes) and two-electron oxidation products TMB_{ox2} (TMB^{2+}).[46] When the concentration of SDS added did not reach the CMC, the surfactant chain stabilized the product cations according to electrostatic gravitation to promote Equation (2) to the left (Figure 3d, left). In the case, SDS promoted oxidation product formation while maintaining the reactants and products in the same solution phase. When the concentration of SDS added exceeded the CMC, a micelle structure was formed. The unique structure enabled the separation of hydrophilic products to the

hydrophilic surface, blocking the interaction between the substrate and product. The entire TMB reaction process was separated by micelles owing to the formation of micellar nanoreactors. The hydrophobic substrate, TMB, was wrapped inside the hydrophobic cavity, and the hydrophilic products ($TMB^{\bullet+}$ and TMB^{2+}) were adsorbed onto the negatively charged outer surface due to electrostatic interactions. That is, the addition of the SDS micelle nanoreactor translated Equation (2) to the left, and the $TMB^{\bullet+}$ formed was transferred to the hydrophilic negatively charged outer layer. The free radical form was unstable and eventually converted to TMB^{2+} by Equation (3) or (4) (Figure 3d, middle). Therefore, adding SDS micellar nanozymes resulted in only yellow two-electron products from the oxidation reaction between TMB and H_2O_2. However, when the surfactant concentration was increased continuously, the "compact" structure of the micellar nanozymes was formed owing to the excessive concentration of surfactant (Figure 3c, right).[47-49] Another reaction substrate, H_2O_2, did not penetrate well into the micelles, which led to a lower effective concentration of reactants in the catalytic region owing to a reduced chance of collisions between reactants. The result was consistent with that in Figure 3a, where there was a tendency for the absorbance of the product at 450 nm to decrease at the same reaction time when the SDS concentration exceeded 15 mM.

$$TMB \xrightarrow{-e^-} TMB^{\bullet+} \quad (1)$$

$$2TMB^{\bullet+} \longleftrightarrow CT\ complex + 2H^+ \quad (2)$$

$$TMB^{\bullet+} \xleftrightarrow{-e^-} TMB^{2+} \quad (3)$$

$$2TMB^{\bullet+} \longleftrightarrow TMB + TMB^{2+} \quad (4)$$

In contrast to the free ROS and bound oxygen intermediates pathways, the SDS micellar nanozymes achieved catalytic acceleration by creating a microenvironment conducive to TMB_{ox2} generation. The catalytic mechanism different from previous nanozymes will bring unique applications in the field of sensing analysis.

Applications of micellar nanozymes for detecting glucose. In nature, most enzymes with peroxygenase activity normally employ a heme cofactor to catalyze peroxidation reactions. A corresponding artificial enzyme was also formed by encapsulating cofactors in micelles or vesicles, which mimic the peptide envelope protecting the catalytic center of the natural enzyme.[50-51] However, the cofactor is susceptible to deactivation by environmental influences.[51-52] Therefore, based on SDS micellar

nanozymes, which relies on the creation of a microenvironment to achieve the catalytic reaction, it remained active even at very high H_2O_2 concentrations. In other words, the cofactor-free micellar nanozymes does not suffer from the phenomenon of "peroxide suicide inactivation",[53] thus enabling the detection of ultra-high concentrations of hydrogen peroxide (0.1-100 mM) (Figure S12a, b). In addition, it has been known that in such a micellar-catalyzed reaction system, hydroxyl radical was the main oxidizing species generated by the autolytic decomposition of H_2O_2. As shown in Figure S13, the response of hydroxyl radicals in the SDS micelle/TMB system was more sensitive than that of the commonly used coumarin for detecting hydroxyl radicals. Hence, the sensitive detection of lower concentrations of H_2O_2 could also be achieved by introducing Fe^{2+}. More hydroxyl radicals were produced via Fenton reaction ($Fe^{2+}$and H_2O_2). As shown in Figure S12c, d (see Supporting Information for details), the Fenton reaction of Fe^{2+} with H_2O_2 significantly improved the sensitivity of the SDS micelle/TMB system for H_2O_2 sensing with limit of detection from millimolar to micromolar.

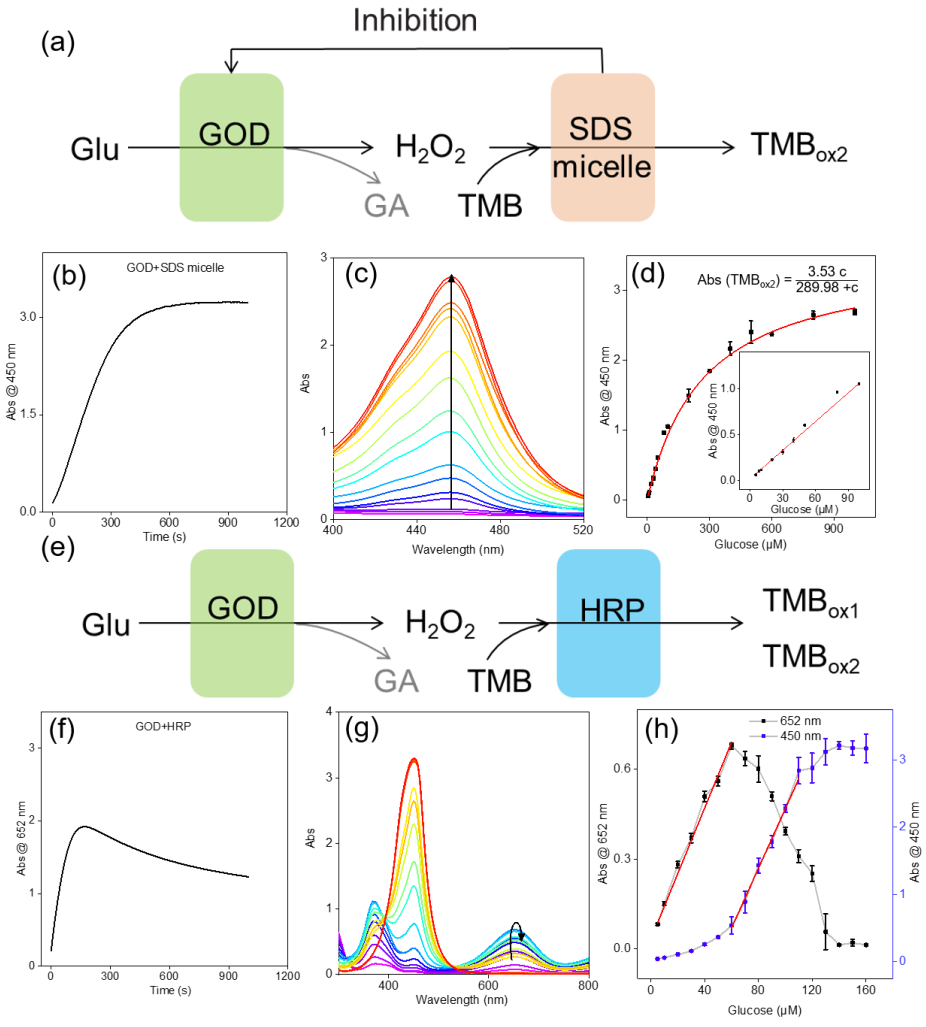

Figure 4. Comparison of SDS and HRP in cascade colorimetric sensors. Schematic for the mechanism of the GOD/SDS micellar (a) and GOD/HRP (d) cascade colorimetric sensors for glucose detection. (Glu: glucose, GOD: glucose oxidase, GA: gluconic acid) (b) Time-dependent UV-vis absorption of TMB_{ox2} (450 nm) catalyzed by SDS (10 mM) with the generation of H_2O_2 during the catalytic oxidation of glucose (100 μM). UV-vis absorption spectra of GOD/SDS micellar system (c) and GOD/HRP system (g) in the presence of different concentrations of glucose. (d) Relationship between absorbance intensity change at 450 nm and glucose concentration. Inset: Calibration curve of absorbance intensity changes at 450 nm versus glucose concentration. (f) Time-dependent UV-vis absorption of TMB_{ox2} (652 nm) catalyzed by HRP (5 μg/mL) with the generation of H_2O_2 during the catalytic oxidation of glucose (100 μM). (h) Calibration curves between absorbance intensity (652 and 450 nm peaks) and glucose concentration. The error bars illustrate the standard deviations of three replicate measurements

Glucose can be oxidized to gluconic acid and H_2O_2 after reacting with GOD and O_2. Thus, the sensitive H_2O_2 response of the present system makes it possible to further establish a platform for detecting glucose, an important biological analyte (Figure 4a). The feasibility of the cascade system (GOD/SDS micellar nanozymes) for glucose sensing was shown in Figure S14. In the absence of the SDS micellar nanozymes, there was only a slight absorption peak at 652 nm (TMB_{ox1}), due to the oxidation of the TMB by the free radicals produced. However, an obvious absorption peak at 450 nm could be observed in the presence of GOD+glucose+TMB+Fe^{2+}+SDS, which indicated that TMB was oxidized toTMB_{ox2} by SDS micellar nanozymes. The results confirmed that the SDS micellar nanozymes was acted as important role in promoting the oxidation of TMB to TMB_{ox2}. Here, SDS had a dual function: a) as a terminator of the glucose oxidation reaction, inhibiting GOD activity and terminating the first step of the reaction (Figure S15).[54] It is known that SDS can destroy the non-covalent bonds of proteins, thereby denaturating proteins and losing their native conformation and function.[55] Therefore, the stability of the signal in the second step was not affected by the continuation of the first step. b) as a micellar nanozymes-building cascade reaction that

initiated the second step of the reaction. Moreover, SDS micellar nanozymes could directly obtain a stable two-electron oxidation product. Hence, the SDS micellar nanozyme not only inhibited GOD activity in the first step of the cascade reaction but also directly drove the two-electron oxidation of TMB, making the output signal more stable and accurate (Figure 4b). Under optimal conditions (Figure S16), the absorbance of oxidized TMB at 450 nm sharply increased with glucose concentration changing from 0 to 1000 μM (Figures 4c and d). Similar to natural enzymes, the molecular recognition mechanism between micellar nanozymes and substrates allowed for datasets that are not aligned along a straight line over a large range of concentrations (5-1000 μM). Along the line, the nonlinear calibration curve (Figure 4d) was fitted under the Michaelis-Menten mechanism.[56] Moreover, a good linear relationship (R^2=0.999) for glucose was also obtained in the concentration range of 0-100 μM (Figure 4d, inset) using the GOD/SDS micelle system. The calculated limit of detection (LOD) of glucose was measured to be 0.73 μM at S/N = 3, which was lower than the glucose threshold value diagnosed as diabetes mellitus and comparable or even superior to those of the reported results, as summarized in Table S1.

Based on the above discussion, the excellent analytical performance of the sensing strategy benefited from the dual function of SDS. For further validation, a cascade catalytic system based on GOD and HRP was designed as a contrast experiment. For the enzyme cascade system based on GOD and HRP (Figure 4e), H_2O_2 would keep producing due to the continuous glucose oxidase reaction. With the increase of H_2O_2 concentration, the product of HRP-catalyzed oxidation of TMB changed and led to signal instability (Figure 4f). As shown in Figure 4g, the catalytic system of GOD/HRP led to the appearance of the two products. The detection range of the GOD/HRP cascade system was divided into two narrower detection ranges (Figure 4h, 5-60 μM at 652 nm with a LOD of 2.1 μM, 60-110 μM at 450 nm with a LOD of 9.7 μM). These multiple variations in the H_2O_2 intermediate generation made the detection of the analyte concentration very unintuitive and convenient. Therefore, compared with GOD/HRP system, GOD/SDS micellar nanozymes system was superior in both detection limit and detection range due to the unique catalytic characteristics of SDS micellar nanozymes.

In order to evaluate the applicability of the proposed method based on the SDS micellar nanozymes as peroxidase mimetics, the present colorimetric method was employed to detect glucose in human serum. Glucose detection in diluted human serum (10, 30, and 100 μM) had a high recovery rate (Table S2), suggesting its practicability in real sample detection. The selectivity of the established glucose-detection system was verified by xylose, trehalose, sucrose, fructose, and galactose as interfering substances. As shown in Figure S17, the detection system was capable of resisting other sugar interferences, demonstrating a good selectivity for glucose detection.

Conclusion

In summary, we reported a reliable colorimetric sensing strategy based on the micellar nanozyme catalyzed oxidation of TMB. The critical factors of micelle-substrate interactions were explored to understand the origin of the unique catalytic ability. Different from the free ROS and bound oxygen intermediates pathways, the SDS micellar nanozymes achieved catalytic acceleration by creating a microenvironment conducive to TMB_{ox2} generation. The special catalytic mechanism and the uniqueness of the catalytic product made SDS micellar nanozymes successfully applied to high concentration H_2O_2 detection and glucose reliable sensing. Due to the properties of SDS micellar nanozymes and the general inhibition of natural enzymes, the micellar nanozyme system avoided the disadvantage of signal instability in natural enzyme systems (HRP and GOD) and achieved reliable and sensitive glucose detection. In addition, the mechanism of action of such micellar nanozymes, which through creates a microenvironment conducive to product generation, will provide new insights into the mechanism of nanozyme catalysis.

References

1. Bornscheuer, U. T.; Huisman, G. W.; Kazlauskas, R. J.; Lutz, S.; Moore, J. C.; Robins, K., Engineering the third wave of biocatalysis. *Nature* **2012,** *485*, 185-194.

2. Wu, S.; Snajdrova, R.; Moore, J. C.; Baldenius, K.; Bornscheuer, U. T., Biocatalysis: Enzymatic Synthesis for Industrial Applications. *Angew. Chem. Int. Ed.* **2020,** *60*, 88-119.

3. Rodriguez-Lopez, J. N.; Lowe, D. J.; Hernandez-Ruiz, J.; Hiner, A. N.; Garcia-Canovas, F.; Thorneley, R. N., Mechanism of reaction of hydrogen peroxide with horseradish peroxidase: identification of intermediates in the catalytic cycle. *J. Am. Chem. Soc.* **2001,** *123*, 11838-11847.

4. Wirstam, M.; Blomberg, M. R.; Siegbahn, P. E., Reaction mechanism of compound I formation in heme peroxidases: a density functional theory study. *J. Am. Chem. Soc.* **1999,** *121*, 10178-10185.

5. Rodríguez-López, J.; Lowe, D. J.; Hernández-Ruiz, J.; Hiner, A.; García-Cánovas, F.; Thorneley, R., Mechanism of reaction of hydrogen peroxide with horseradish peroxidase: identification of intermediates in the catalytic cycle. *J. Am. Chem. Soc.* **2001,** *123*, 11838.

6. Yang, S.; Jia, W.-Z.; Qian, Q.-Y.; Zhou, Y.-G.; Xia, X.-H., Simple Approach for Efficient Encapsulation of Enzyme in Silica Matrix with Retained Bioactivity. *Anal. Chem.* **2009,** *81*, 3478-3484.

7. Zhu, Y.-C.; Xu, Y.-T.; Xue, Y.; Fan, G.-C.; Zhang, P.-K.; Zhao, W.-W.; Xu, J.-J.; Chen, H.-Y., Three-Dimensional CdS@Carbon Fiber Networks: Innovative Synthesis and Application as a General Platform for Photoelectrochemical Bioanalysis. *Anal. Chem.* **2019,** *91*, 6419-6423.

8. Li, X.; Du, Y.; Wang, H.; Ma, H.; Wu, D.; Ren, X.; Wei, Q.; Xu, J.-J., Self-Supply of H_2O_2 and O_2 by Hydrolyzing CaO_2 to Enhance the Electrochemiluminescence of Luminol Based on a Closed Bipolar Electrode. *Anal. Chem.* **2020,** *92*, 12693-12699.

9. Yang, J.; Li, X.; Jiang, B.; Yuan, R.; Xiang, Y., In Situ-Generated Multivalent Aptamer Network for Efficient Capture and Sensitive Electrochemical Detection of Circulating Tumor Cells in Whole Blood. *Anal. Chem.* **2020,** *92*, 7893-7899.

10. Sun, L.-P.; Huang, Y.; Huang, T.; Yuan, Z.; Lin, W.; Sun, Z.; Yang, M.; Xiao, P.; Ma, J.; Wang, W., Optical microfiber reader for enzyme-linked immunosorbent assay. *Anal. Chem.* **2019,** *91*, 14141-14148.

11. Zhang, Y.; Zhang, B.; Ye, X.; Yan, Y.; Huang, L.; Jiang, Z.; Tan, S.; Cai, X., Electrochemical immunosensor for interferon-γ based on disposable ITO detector and HRP-antibody-conjugated nano gold as signal tag. *Materials Science and Engineering: C* **2016,** *59*, 577-584.

12. Wu, S.; Sun, Z.; Peng, Y.; Han, Y.; Li, J.; Zhu, S.; Yin, Y.; Li, G., Peptide-functionalized metal-organic framework nanocomposite for ultrasensitive detection of secreted protein acidic and rich in cysteine with practical application. *Biosens. Bioelectron.* **2020,** *169*, 112613.

13. Ma, C. B.; Xu, Y.; Wu, L.; Wang, Q.; Zheng, J. J.; Ren, G.; Wang, X.; Gao, X.; Zhou, M.; Wang, M.; Wei, H., Guided Synthesis of a Mo/Zn Dual Single-Atom Nanozyme with Synergistic Effect and Peroxidase-like Activity. *Angew. Chem. Int. Ed.* **2022,** *61*, e202116170.

14. Ji, S.; Jiang, B.; Hao, H.; Chen, Y.; Dong, J.; Mao, Y.; Zhang, Z.; Gao, R.; Chen, W.; Zhang, R.; Liang, Q.; Li, H.; Liu, S.; Wang, Y.; Zhang, Q.; Gu, L.; Duan, D.; Liang, M.; Wang, D.; Yan, X.; Li, Y., Matching the kinetics of natural enzymes with a single-atom iron nanozyme. *Nat. Catal.* **2021,** *4*, 407-417.

15. Gao, L.; Zhuang, J.; Nie, L.; Zhang, J.; Zhang, Y.; Gu, N.; Wang, T.; Feng, J.; Yang, D.; Perrett, S.; Yan, X., Intrinsic peroxidase-like activity of ferromagnetic nanoparticles. *Nat. Nanotechnol.* **2007,** *2*, 577-583.

16. Yu, L.; Chang, J.; Zhuang, X.; Li, H.; Hou, T.; Li, F., Two-Dimensional Cobalt-Doped Ti_3C_2 MXene Nanozyme-Mediated Homogeneous Electrochemical Strategy for Pesticides Assay Based on In Situ Generation of Electroactive Substances. *Anal. Chem.* **2022,** *94*, 3669-3676.

17. Hu, W. C.; Younis, M. R.; Zhou, Y.; Wang, C.; Xia, X. H., In situ fabrication of ultrasmall gold nanoparticles/2D MOFs hybrid as nanozyme for antibacterial therapy. *Small* **2020,** *16*, 2000553.

18. Zhen, W.; Liu, Y.; Wang, W.; Zhang, M.; Hu, W.; Jia, X.; Wang, C.; Jiang, X.,

Specific “Unlocking” of a Nanozyme-Based Butterfly Effect To Break the Evolutionary Fitness of Chaotic Tumors. *Angew. Chem. Int. Ed.* **2020,** *59*, 9491-9497.

19. Ruan, X.; Liu, D.; Niu, X.; Wang, Y.; Simpson, C. D.; Cheng, N.; Du, D.; Lin, Y., 2D Graphene Oxide/Fe-MOF Nanozyme Nest with Superior Peroxidase-Like Activity and Its Application for Detection of Woodsmoke Exposure Biomarker. *Anal. Chem.* **2019,** *91*, 13847-13854.

20. Zhang, C.; Xue, X.; Luo, Q.; Li, Y.; Yang, K.; Zhuang, X.; Jiang, Y.; Zhang, J.; Liu, J.; Zou, G.; Liang, X.-J., Self-Assembled Peptide Nanofibers Designed as Biological Enzymes for Catalyzing Ester Hydrolysis. *ACS Nano* **2014,** *8*, 11715-11723.

21. Liu, Q.; Wang, H.; Shi, X.; Wang, Z.-G.; Ding, B., Self-Assembled DNA/Peptide-Based Nanoparticle Exhibiting Synergistic Enzymatic Activity. *ACS Nano* **2017,** *11*, 7251-7258.

22. Ren, F.; Hua, M.; Yang, Z.; Wei, J., Self-assembled artificial enzyme from hybridized porous organic cages and iron oxide nanocrystals. *J. Colloid Interface Sci.* **2022,** *621*, 331-340.

23. Liu, S.; Du, P.; Sun, H.; Yu, H.-Y.; Wang, Z.-G., Bioinspired Supramolecular Catalysts from Designed Self-Assembly of DNA or Peptides. *ACS Catal.* **2020,** *10*, 14937-14958.

24. Mikolajczak, D. J.; Berger, A. A.; Koksch, B., Catalytically Active Peptide–Gold Nanoparticle Conjugates: Prospecting for Artificial Enzymes. *Angew. Chem. Int. Ed.* **2020,** *59*, 8776-8785.

25. Liu, Q.; Wan, K.; Shang, Y.; Wang, Z.-G.; Zhang, Y.; Dai, L.; Wang, C.; Wang, H.; Shi, X.; Liu, D.; Ding, B., Cofactor-free oxidase-mimetic nanomaterials from self-assembled histidine-rich peptides. *Nat. Mater.* **2020,** *20*, 395-402.

26. Meng, X. G.; Guo, Y.; Hu, C. W.; Zeng, X. C., Mimic models of peroxidase--kinetic studies of the catalytic oxidation of hydroquinone by H_2O_2. *J. Inorg. Biochem.* **2004,** *98*, 2107-2113.

27. Sorrenti, A.; Illa, O.; Ortuño, R. M., Amphiphiles in aqueous solution: well beyond a soap bubble. *Chem. Soc. Rev.* **2013,** *42*, 8200.

28. MacFarlane, L.; Zhao, C.; Cai, J.; Qiu, H.; Manners, I., Emerging applications

for living crystallization-driven self-assembly. *Chem. Sci.* **2021,** *12*, 4661-4682.

29. La Sorella, G.; Strukul, G.; Scarso, A., Recent advances in catalysis in micellar media. *Green Chem.* **2015,** *17*, 644-683.

30. Banerjee, M.; Panjikar, P. C.; Bhutia, Z. T.; Bhosle, A. A.; Chatterjee, A., Micellar nanoreactors for organic transformations with a focus on "dehydration" reactions in water: A decade update. *Tetrahedron* **2021,** *88*, 132142.

31. Mikuka, P.; Veea, Z., Effect of complexones and tensides on selectivity of nitrogen dioxide determination in air with a chemiluminescence aerosol detector. *Anal. Chim. Acta* **2000,** *410*, 159-165.

32. Li, M.; Su, H.; Tu, Y.; Shang, Y.; Liu, Y.; Peng, C.; Liu, H., Development and Application of an Efficient Medium for Chromogenic Catalysis of Tetramethylbenzidine with Horseradish Peroxidase. *ACS Omega* **2019,** *4*, 5459-5470.

33. Sobhani, S.; Vafaee, A., Micellar solution of sodium dodecyl sulfate (SDS) catalyzes Kabacknik-Fields reaction in aqueous media. *Synthesis* **2009,** *2009*, 1909-1915.

34. Frias Batista, L. M.; Meader, V. K.; Romero, K.; Kunzler, K.; Kabir, F.; Bullock, A.; Tibbetts, K. M., Kinetic Control of $[AuCl_4]^-$ Photochemical Reduction and Gold Nanoparticle Size with Hydroxyl Radical Scavengers. *The Journal of Physical Chemistry B* **2019,** *123*, 7204-7213.

35. Gao, L.; Zhuang, J.; Nie, L.; Zhang, J.; Zhang, Y.; Gu, N.; Wang, T.; Feng, J.; Yang, D.; Perrett, S.; Yan, X., Intrinsic peroxidase-like activity of ferromagnetic nanoparticles. *Nat. Nanotechnol.* **2007,** *2*, 577-583.

36. Chen, X.; Zhao, L.; Wu, K.; Yang, H.; Zhou, Q.; Xu, Y.; Zheng, Y.; Shen, Y.; Liu, S.; Zhang, Y., Bound oxygen-atom transfer endows peroxidase-mimic M–N–C with high substrate selectivity. *Chem. Sci.* **2021,** *12*, 8865-8871.

37. Kunitake, T.; Shinkai, S., Catalysis by micelles, membranes and other aqueous aggregates as models of enzyme action. *Adv. Phys. Org. Chem.* **1980,** *17*, 435-487.

38. 周晴中; 文重, 胶束催化与胶束模拟酶研究. *化学通报* **1987,** *5*, 21-26+6.

39. Hassan, P.; Raghavan, S. R.; Kaler, E. W., Microstructural changes in SDS

micelles induced by hydrotropic salt. *Langmuir* **2002,** *18*, 2543-2548.

40. Schäfer, K.; Kolli, H. B.; Killingmoe Christensen, M.; Bore, S. L.; Diezemann, G.; Gauss, J.; Milano, G.; Lund, R.; Cascella, M., Supramolecular Packing Drives Morphological Transitions of Charged Surfactant Micelles. *Angew. Chem. Int. Ed.* **2020,** *59*, 18591-18598.

41. Zana, R.; Kaler, E. W., *Giant micelles: properties and applications*. CRC press: 2007; Vol. 140.

42. Jensen, G. V.; Lund, R.; Gummel, J.; Narayanan, T.; Pedersen, J. S., Monitoring the Transition from Spherical to Polymer-like Surfactant Micelles Using Small-Angle X-Ray Scattering. *Angew. Chem. Int. Ed.* **2014,** *53*, 11524-11528.

43. Sar, P.; Ghosh, A.; Saha, R.; Saha, B., Micellar effect on pentavalent vanadium oxidation of formaldehyde to formic acid in aqueous acid media at room temperature. *Res. Chem. Intermed.* **2015,** *41*, 5331-5352.

44. Rakshit, A.; Chowdhury, S.; Acharjee, A.; Datta, I.; Dome, K.; Biswas, S.; Bhattacharyya, S. S.; Saha, B., Hetero-aromatic N-base-promoted oxidation of 4-chlorobenzyl alcohol by Cr (VI) in micellar media. *Res. Chem. Intermed.* **2020,** *46*, 2559-2578.

45. Nkole, I.; Abdulsalam, S.; Ibrahim, I.; Arthur, D., Micellar effect on electron transfer reaction of 2-(hydroxyethyl) ethylenediaminetriacetatoiron (III) complex with thiocarbonate ion: kinetic model. *Chem. Afr.* **2021,** *4*, 525-533.

46. Misono, Y.; Ohkata, Y.; Morikawa, T.; Itoh, K., Resonance Raman and absorption spectroscopic studies on the electrochemical oxidation processes of 3, 3′, 5, 5′-tetramethylbenzidine. *J. Electroanal. Chem.* **1997,** *436*, 203-212.

47. Paleologos, E. K.; Vlessidis, A. G.; Karayannis, M. I.; Evmiridis, N. P., On-line sorption preconcentration of metals based on mixed micelle cloud point extraction prior to their determination with micellar chemiluminescence. *Anal. Chim. Acta* **2003,** *477*, 223-231.

48. Zhao, D.; Zhang, G.; Jiang, T.; Deng, Z.; Wu, Y., Flow-injection chemiluminescence method for determination of critical micelle concentration of surfactants. *Int. J. Environ. Anal. Chem.* **2015,** *95*, 980-988.

49. Danov, K. D.; Kralchevsky, P. A.; Stoyanov, S. D.; Cook, J. L.; Stott, I. P., Analytical modeling of micelle growth. 1. Chain-conformation free energy of binary mixed spherical, wormlike and lamellar micelles. *J. Colloid Interface Sci.* **2019,** *547*, 245-255.

50. Moosavi-Movahedi, A. A.; Semsarha, F.; Heli, H.; Nazari, K.; Ghourchian, H.; Hong, J.; Hakimelahi, G. H.; Saboury, A. A.; Sefidbakht, Y., Micellar histidinate hematin complex as an artificial peroxidase enzyme model: Voltammetric and spectroscopic investigations. *Colloids Surf. A Physicochem. Eng. Asp.* **2008,** *320*, 213-221.

51. Gharibi, H.; Moosavi-Movahedi, Z.; Javadian, S.; Nazari, K.; Moosavi-Movahedi, A. A., Vesicular Mixed Gemini−SDS−Hemin−Imidazole Complex as a Peroxidase-Like Nano Artificial Enzyme. *The Journal of Physical Chemistry B* **2011,** *115*, 4671-4679.

52. Ahmadzade Kermani, H.; Shockravi, A.; Moosavi-Movahedi, Z.; Khalafi-Nezhad, A.; Behrouz, S.; Tsai, F.-Y.; Hakimelahi, G.; Seyedarabi, A.; Moosavi-Movahedi, A., A surfactant–heme–sulfonyl imidazole system as a nano-artificial enzyme. *J. Iran. Chem. Soc.* **2013,** *10*, 961-968.

53. Bratton, M. R.; Pressler, M. A.; Hosler, J. P., Suicide inactivation of cytochrome c oxidase: catalytic turnover in the absence of subunit III alters the active site. *Biochemistry* **1999,** *38*, 16236-16245.

54. Otzen, D., Protein–surfactant interactions: A tale of many states. *Biochimica et Biophysica Acta (BBA) - Proteins and Proteomics* **2011,** *1814*, 562-591.

55. Lau, F. W.; Bowie, J. U., A Method for Assessing the Stability of a Membrane Protein. *Biochemistry* **1997,** *36*, 5884-5892.

56. Hong, Q.; Shen, Y.; Liu, S.; Zhang, Y., Re-Examination of Plotting Analytical Response against Different Forms of Concentration. *Anal. Chem.* **2021,** *93*, 11910-11914.